Cerebral monitoring during carotid endarterectomy using near-infrared diffuse optical spectroscopies and electroencephalogram

Cerebral monitoring during carotid endarterectomy using near-infrared diffuse optical spectroscopies and electroencephalogram

Yu Shang[1]**, Ran Cheng**[1]**, Lixin Dong**[1]**, Stephen J Ryan**[2]**, Sibu P Saha**[3] **and Guoqiang Yu**[1]

[1] Center for Biomedical Engineering, University of Kentucky, KY, USA
[2] Department of Neurology, University of Kentucky, KY, USA
[3] Division of Cardiothoracic Surgery, University of Kentucky, KY, USA

E-mail: guoqiang.yu@uky.edu

Abstract

Intraoperative monitoring of cerebral hemodynamics during carotid endarterectomy (CEA) provides essential information for detecting cerebral hypoperfusion induced by temporary internal carotid artery (ICA) clamping and post-CEA hyperperfusion syndrome. This study tests the feasibility and sensitivity of a novel dual-wavelength near-infrared diffuse correlation spectroscopy technique in detecting cerebral blood flow (CBF) and cerebral oxygenation in patients undergoing CEA. Two fiber-optic probes were taped on both sides of the forehead for cerebral hemodynamic measurements, and the instantaneous decreases in CBF and electroencephalogram (EEG) alpha-band power during ICA clamping were compared to test the measurement sensitivities of the two techniques. The ICA clamps resulted in significant CBF decreases ($-24.7 \pm 7.3\%$) accompanied with cerebral deoxygenation at the surgical sides ($n = 12$). The post-CEA CBF were significantly higher ($+43.2 \pm 16.9\%$) than the pre-CEA CBF. The CBF responses to ICA clamping were significantly faster, larger and more sensitive than EEG responses. Simultaneous monitoring of CBF, cerebral oxygenation and EEG power provides a comprehensive evaluation of cerebral physiological status, thus showing potential for the adoption of acute interventions (e.g., shunting, medications) during CEA to reduce the risks of severe cerebral ischemia and cerebral hyperperfusion syndrome.

(Some figures in this article are in colour only in the electronic version)

1. Introduction

Approximately 20% of ischemic strokes are caused by extracranial internal carotid artery (ICA) stenosis (Chaturvedi *et al* 2005, Chang *et al* 1995). Carotid endarterectomy (CEA) is the most

frequently used surgical intervention for restoration of the blood circulation by removing the blockage from the carotid artery, thus reducing the stroke risk (Chaturvedi *et al* 2005, Plestis *et al* 1997, Rowed *et al* 2004). During CEA, the common, external and internal carotid arteries are temporarily clamped for removal of the atheromatous plaques in the inner lining of the carotid artery. The ICA clamping, if without temporary shunting (a temporary bypass connecting the sections below and above blockage for establishment of blood flow in clamped artery) to the brain, may lead to cerebral ischemia and hypoxia. However, the shunting itself may induce embolic events leading to perioperative stroke (Bond *et al* 2003, Ackerstaff *et al* 1995). The use of shunting during ICA clamping is usually selected by surgeons based on the real-time monitoring of brain physiological status (e.g., electroencephalographic monitoring) associated with cerebral *hypoperfusion* during surgery (Moritz *et al* 2007, Blume *et al* 1986, Cursi *et al* 2005). Moreover, real-time monitoring of cerebral perfusion may help in making decisions for adopting acute medications for reducing the risk of cerebral *hyperperfusion* syndrome (CHS): a cause of neurological dysfunction after CEA (Adhiyaman and Alexander 2007).

Currently, techniques for direct or indirect monitoring of cerebral perfusion during CEA at the bedside of surgical rooms include electroencephalography (EEG) (Blume *et al* 1986, Cursi *et al* 2005, Hirofumi *et al* 2003, Jansen *et al* 1993, Plestis *et al* 1997, Rowed *et al* 2004), somatosensory-evoked potential (SEP) (Friedell *et al* 2008, Rowed *et al* 2004, Moritz *et al* 2007), transcranial Doppler sonography (TCD) (Jansen *et al* 1993, Rowed *et al* 2004, Ackerstaff *et al* 1995, Moritz *et al* 2007, Belardi *et al* 2003), stump pressure (SP) (Moritz *et al* 2007, Belardi *et al* 2003) and Xe^{133} technique (Sundt *et al* 1981). Among these techniques, EEG and SEP record the cerebral functional state (Franceschini *et al* 2008, Moritz *et al* 2007) that does not necessarily reflect the cerebral perfusion. TCD and SP detect blood flow or blood pressure in large cerebral vessels which may not be consistent with cerebral blood flow (CBF) in microvasculature (Edlow *et al* 2010). Although the Xe^{133} technique can measure CBF in microvasculature, the invasive and complex nature of injecting radioactive isotopes in artery limits its wide use during surgery.

Near-infrared diffuse optical spectroscopy (NIRS) offers a noninvasive, rapid, portable and low-cost alternative for direct monitoring of cerebral tissue oxygenation in microvasculature (Fantini *et al* 1999, Boas *et al* 2001, Culver *et al* 2005, Hebden *et al* 2004, Everdell *et al* 2005, Tian *et al* 2009, Franceschini *et al* 2006). The difference between major tissue chromophores in near-infrared (NIR) absorption spectra allows for the measurement of oxygenated and de-oxygenated hemoglobin concentrations, total hemoglobin concentration and blood oxygen saturation. NIRS has also been incorporated with EEG for concurrently detecting cerebral oxygenation and brain waves in premature infants (Roche-Labarbe *et al* 2007), healthy adults (Cooper *et al* 2009b, Rovati *et al* 2007), and tissue-like phantoms (Cooper *et al* 2009a). Applications of an NIR tissue oximeter during CEA have demonstrated that severe cerebral ischemia is associated with 5–25% decline in cerebral blood oxygen saturation (Pennekamp *et al* 2009). However, the NIR tissue oximeter does not directly measure CBF.

NIR diffuse correlation spectroscopy (DCS) is an emerging technique capable of directly measuring CBF in healthy and diseased brains (Durduran *et al* 2004, 2009, 2010, Gagnon *et al* 2008 Cheung *et al* 2001, Culver *et al* 2003, Li *et al* 2008, Zhou *et al* 2009, Roche-Labarbe *et al* 2010, Zirak *et al* 2010). DCS utilizes rapid temporal fluctuations of NIR light intensity to directly detect the motion of moving scatterers (e.g., red blood cells) in the microvasculature of biological tissues. Measurements of blood flow variations by DCS in various organs and tissues have been compared and validated to other standards, including power Doppler ultrasound (Yu *et al* 2005b), laser Doppler (Durduran 2004), Xenon-CT (Kim *et al* 2010), Doppler ultrasound (Buckley *et al* 2009, Roche-Labarbe *et al* 2010), fluorescent microsphere

measurement (Zhou *et al* 2009), and perfusion MRI (Yu *et al* 2007). DCS offers several attractive new features for blood flow measurement, such as noninvasiveness, high temporal resolution (up to several milliseconds) (Dietsche *et al* 2007), portability and relatively large penetration depth (up to several centimeters) (Durduran *et al* 2004, Li *et al* 2005).

In some of the previous studies described above, DCS was combined with the NIR tissue oximeter in hybrid instruments to simultaneously measure both blood flow and oxygenation which allows an estimation of tissue oxygen metabolism (Zhou *et al* 2007, Yu *et al* 2005a, Roche-Labarbe *et al* 2010). However, the combination of DCS flowmeter and NIR tissue oximeter made the hybrid instruments large and expensive. Recently, we developed a truly portable, easy-to-use and relatively inexpensive diffuse optical device based on DCS technology (namely *DCS flow-oximeter*) for simultaneous monitoring of tissue blood flow and oxygenation (Shang *et al* 2009). DCS flow-oximeter measurements of blood oxygenation changes have been validated against a commercial tissue oximeter (Imagent, ISS Inc.) (Shang *et al* 2009). Being truly portable (dimensions: $8'' \times 12'' \times 18''$), the DCS flow-oximeter is suitable for bedside monitoring of CBF and oxygenation in clinic, thus providing a comprehensive evaluation of cerebral physiological status.

This study aims to test the capability of DCS flow-oximeter in detecting cerebral hypoperfusion and hypoxia during ICA clamping as well as post-CEA hyperperfusion in surgical rooms. To the best of our knowledge, there have been no published reports of simultaneous measurements of CBF and cerebral oxygenation in microvasculature during CEA. Since EEG was applied in our patient population by the surgeon to detect the severe cerebral hypoperfusion for shunting selection, we compared the CBF variations measured by the DCS flow-oximeter with the changes of EEG power spectra to test the sensitivity of optical measurements in the evaluation of cerebral hemodynamics during CEA.

2. Methods

2.1. Patient characteristics and surgical procedures

Eleven patients with carotid stenosis and undergoing CEA participated in this study with the signed consents approved by the University of Kentucky Institutional Review Board (IRB). The stenoses caused by plaques inside the ICA were identified by duplex Doppler ultrasound, magnetic resonance (MR) and/or computed tomography (CT) angiography. Table 1 lists patient demographics, carotid stenosis percentages at the surgical and opposite (control) sides, and ICA clamping duration. The left or right side for each individual surgery was selected primarily based on the severity of carotid stenosis. However, patient 4 received CEA at the left side with 80% stenosis rather than the right side with 100% stenosis. In fact, CEA for 100% stenosis is not recommended since the surgical benefits to total ICA occlusion are insufficient and the surgeries are associated with a high risk of preoperative stroke (Matic *et al* 2009, Bowen *et al* 1997). Note that one patient underwent CEA twice at the right and left sides, respectively, on two different dates with an interval of 67 days. This patient was assigned two consequence numbers (5 and 6) for differentiating the right and left CEA. In total, 12 CEA procedures were monitored in this study.

The patients were placed under general endotracheal anesthesia. Using a standard sterile technique, an incision was made on the side with severe ICA stenosis along the anterior border of sternomastoid muscle and was deepened on subcutaneous tissue and platysma. After the placement of a self-retaining retractor and ligation of common facial vein, the carotid sheath was opened and common, external and internal carotid arteries were exposed and clamped sequentially using vascular clamps. Patients were given 5000 units of heparin prior
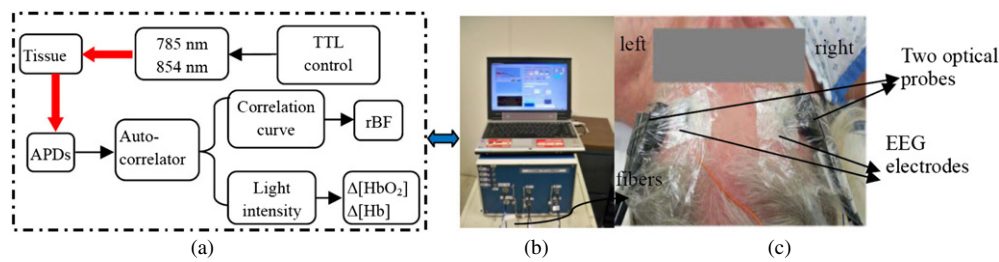
Figure 1. DCS flow-oximeter for cerebral blood flow (CBF) and cerebral oxygenation measurements. (a) Diagram of the DCS flow-oximeter; (b) photograph of the DCS flow-oximeter; (c) two fiber-optic probes taped on the left and right sides of the patient's forehead. Note that this photograph was taken before wrapping the Velcro strap on top of the optical probes to clarify the placement of DCS probes on head.

Table 1. Patient characteristics.

Patient	Age	Gender	Percentage of carotid stenosis at surgical side	Percentage of carotid stenosis at control side	Clamping duration (min)
1	74	M	~90% (R)	30% (L)	17.9
2	34	F	<50% (L)	40% (R)	12.0
3	79	M	>80% (R)	>60% (L)	20.2
4	60	M	~80% (L)	100% (R)	12.8
5	57	F	>90% (R)	85% (L)	17.5
6	57	F	80–90% (L)	<30% (R)	24.2
7	60	M	~76% (R)	<30% (L)	18.0
8	52	M	~80% (L)	20% (R)	15.3
9	65	M	80–85% (L)	10% (R)	18.5
10	81	M	95–98% (R)	65% (L)	18.9
11	72	F	~75% (R)	25% (L)	23.6
12	82	M	90–95% (R)	<50% (L)	18.3

to clamping. Arteriotomy was made by opening the common carotid artery and extending the incision onto the ICA. Endarterectomy was then carried out by a standard technique. An expert electroencephalographer visually monitored the EEG signals (see section 2.2) throughout ICA clamping. Based on the visual inspections, there were no significant changes in concomitant EEG signals during ICA clamping in all patients presented in this study; thus no patients received shunting during CEA. After endarterectomy, all clamps were released and the incision was closed in layers.

2.2. Near-infrared DCS tissue flow-oximeter and EEG system

A custom-designed dual-wavelength DCS flow-oximeter (see figure 1) was used for continuous monitoring of CBF and cerebral oxygenation throughout CEA. Details about the DCS flow-oximeter can be found elsewhere (Shang *et al* 2009). Briefly, long-coherence (>5 m) NIR light emitted from two laser diodes (785 and 854 nm, 100 and 120 mw, Crystalaser Inc., USA) enters the tissue alternately via two multimode source fibers (diameter = 200 μm).

The scattered light through the tissue is collected by a single-mode detector fiber (diameter = 5.6 μm) connected to an avalanche photodiode (APD, Pacer Components Inc., UK). The distance between the fibers of the laser source (S) and the APD detector (D) is 2.5 cm. The light intensity fluctuation within a single speckle area of tissue ($\sim$25 ($\pi \times (5.6/2)^2$) μm^2), detected by the APD, is sensitive to the motion of moving scatterers in tissue (e.g., moving red blood cells). An autocorrelator board (www.correlator.com, USA) takes the output of APD and computes the light intensity temporal autocorrelation function. From the normalized intensity autocorrelation function, the electric field temporal autocorrelation function $G_1(\tau)$ is derived, which satisfies the correlation diffusion equation in highly scattering media (Boas *et al* 1995, Boas and Yodh 1997). The exact form of the correlation diffusion equation depends on the nature and heterogeneity of the scatterer motion. For the case of diffusive motion, the normalized electric field temporal autocorrelation function $g_1(\tau)$ decays at an early time approximately exponentially in τ (delay time). Relative blood flow (rBF) is thus extracted by fitting the autocorrelation curve whose decay rate depends on a parameter α (which is proportional to the tissue blood volume fraction), and on the motion of the red blood cells (Cheung *et al* 2001, Yu *et al* 2005a, 2005b, Boas *et al* 1995). The two wavelength measurements (785 and 854 nm) generate two flow curves (Shang *et al* 2009).

The oxygenation information is extracted from data obtained by recording the average light intensities at two wavelengths (785 and 854 nm) detected by the APD. The wavelengths were chosen based on the lasers available, and optimization of wavelengths (Strangman *et al* 2003) will be the subject of future work. The changes of oxygenated hemoglobin concentration (Δ[HbO$_2$]) and deoxygenated hemoglobin concentration (Δ[Hb]) relative to their baseline values (determined before physiological changes) are calculated using a 'differential pathlength method' (Strangman *et al* 2003, Song *et al* 2005), based on the modified Beer–Lambert law. In this method, the standard Beer–Lambert law is modified to account for the lengthening of the mean photon pathlength due to tissue scattering. A differential pathlength factor (DPF) is introduced, which is the ratio of the mean photon pathlength to the physical separation of the source and detector. The detected time-course changes in light intensities at two wavelengths depend on extinction coefficients and DPF values at the working wavelengths as well as hemoglobin concentration changes (Δ[HbO$_2$] and Δ[Hb]) of the measured tissue. The extinction coefficients and DPF values are determined based on the literatures (Duncan *et al* 1995, Kim *et al* 2005).

A 16-channel EEG system (XLTEK, Excel-Tech Ltd, Canada) was used to continuously monitor brain waves during CEA. Nineteen electrodes (including 16 active electrodes and 3 reference electrodes) were placed around the scalp based on 10–20 International System (Fisch 1999). The electrode placed on a specific location of scalp probed the averaged field potential created by the cortical neurons in that particular area of the brain (Kaiser 2005).

2.3. Optical and EEG measurements

Two fiber-optic probes containing source and detector fibers were taped on the surgical (with temporary ICA clamping during CEA) and control (without ICA clamping) sides of the forehead (see figure 1) before surgery using sterile transparent dressing (Tegaderm™, 3M Health Care, USA). A Velcro strap was then employed across the forehead to tightly fix both probes and minimize the influence of room light on optical measurements. The two optical probes were connected to two DCS flow-oximeter devices for simultaneous monitoring of CBF and cerebral tissue oxygenation at both sides. The sampling time for a complete frame of flow and oxygenation measurements was 2.4 s. Note that one patient underwent two separate CEA surgeries on different dates, and received temporary ICA clamping at only one side

during each CEA. This patient was assigned two consequential numbers (5 and 6), and the unclamped side during each CEA was used as the control side for comparison.

The 16-channel EEG signals were obtained from FP1-F3, F3-C3, C3-P3, P3-O1, FP1-F7, F7-T7, T7-P7, P7-O1 positions on the left hemisphere, and FP2-F4, F4-C4, C4-P4, P4-O2, FP2-F8, F8-T8, T8-P8, P8-O2 positions on the right hemisphere (Fisch 1999). The sampling rate of the system was 500 Hz, and a band-pass filter (0.1–100 Hz) was implemented to reduce noises at low and high frequencies.

2.4. EEG data analysis: instantaneous changes during ICA clamping

A previously established power spectral method (Cursi *et al* 2005, Blume *et al* 1986) is used to quantify the instantaneous changes in EEG signals during ICA clamping. Briefly, 2 s EEG data (1000 data points at 500 Hz sampling rate) centered at time t from each of 16 channels are detrended as one series. After being preprocessed by a Hanning window to reduce the effect of spectral leakage, each series is transformed into a frequency domain by Fast Fourier Transform (FFT), from which the power spectrum at 8–15 Hz bandwidth is obtained. The reduction in 8–15 Hz EEG spectral power during ICA clamping compared to the baseline value indicates a decline in alpha-band brain activity, which is believed to be closely related to cerebral ischemia (Cursi *et al* 2005, Mariucci *et al* 2003, Blume *et al* 1986). The consecutive series of the 2 s power spectra are then smoothed with Welch's method (Oppenheim and Schafer 1975) through averaging 10 series of power spectra data. By averaging the 8-channel power spectra on left and right hemispheres, respectively, the function of spectral power $P(t)$ at the time t is acquired for each hemisphere.

To evaluate instantaneous changes of EEG signals during ICA clamping, the EEG desynchronization function $D(t)$ is defined as $D(t) = 100\% \times (P(t) - P_0)/P_0$. Here $D(t)$ represents the percentage change of spectral power at time t, when compared to 1 min averaged pre-clamping power P_0 (the reference power). A slope of $D(t)$ during the first 30 s clamping period, $S = (D(t_0 + 30) - D(t_0))/30$, is then calculated to quantify the instantaneous EEG responses to the ICA clamping, since most of EEG changes occur within 30 s after the beginning of clamping (Plestis *et al* 1997). Here t_0 is the beginning time of arterial clamping. The minimum of $D(t)$ during the entire period of clamping is defined as D-index, representing the most severe cerebral hypoperfusion during ICA clamping. The period from the beginning of clamping (t_0) to the time of $D(t)$ attaining its minimum (D-index) is defined as time-to-minimum.

2.5. Optical data analysis

2.5.1. Individual hemodynamic responses throughout CEA. The optical measurements using a source–detector (S–D) separation of 2.5 cm permit NIR light to penetrate ∼1.25 cm into the tissue, allowing for the detection of cerebral hemodynamics in adult cortex (Kim *et al* 2010). The uses of 2.5 cm S–D separation for detection of CBF and cerebral oxygenation have been demonstrated and validated in various human studies (Edlow *et al* 2010, Durduran *et al* 2004, 2009, Li *et al* 2005, Kim *et al* 2010). For example, Kim *et al* (2010) have recently demonstrated that the CBF obtained from the 2.5 cm S–D separation of DCS measurement agreed well with the CBF in adult cortex detected by Xenon-Enhanced CT. Note however, even at this relatively large S–D separation (2.5 cm), there are always some contributions to the cortex signal from the overlaying tissues (skin and skull), i.e., the partial volume effects (Durduran *et al* 2004). In order to precisely extract cerebral hemodynamic information, measurements with multiple source–detector separations and multi-layer theoretical models

are required (Kienle and Glanzmann 1999, Farrell *et al* 1998, van Beekvelt *et al* 2001), which will be the subject of future work.

Since DCS flow signals are not sensitive to variation in the wavelength (Shang *et al* 2009), CBF data obtained from one wavelength (785 nm) are presented in this study. Cerebral oxygenation changes are extracted by measuring the light intensity changes at two wavelengths (785 and 854 nm). Individual time traces for relative changes in CBF and oxygenation during CEA are calculated and presented. The relative CBF (rCBF) is denoted as the CBF percentage relative to its baseline value (assigned to be 100%). The $\Delta[HbO_2]$ and $\Delta[Hb]$ represent the changes of oxygenated and deoxygenated hemoglobin concentrations relative to their baseline values (assigned to be zero).

2.5.2. Averaged hemodynamic changes throughout CEA.   In order to evaluate hemodynamic and EEG changes during ICA clamping and compare with previous studies (Cursi *et al* 2005), the 1 min hemodynamic data (rCBF, $\Delta[HbO_2]$, $\Delta[Hb]$) right before clamping are averaged as the pre-clamping baselines, which are consistent with the data analysis used in previous studies. The mean hemodynamic values during the entire period of ICA clamping are then compared to these pre-clamping baselines for the evaluation of cerebral ischemia/hypoxia during ICA clamping. The post-CEA hemodynamic data are averaged for 5 min and compared to the 5 min averaged pre-CEA baselines for investigating the CEA-created hemodynamic changes.

2.5.3. Instantaneous CBF changes during ICA clamping.   To evaluate instantaneous CBF changes during ICA clamping and compare them to the brain activity (EEG) changes, the same method used for EEG spectral power ($P(t)$) (see section 2.4) is applied to the CBF data analysis, resulting in derivative CBF outcomes of $D(t)$, slope (S), D-index and time-to-minimum.

3. Results

3.1. Individual cerebral hemodynamic changes throughout CEA

The data analysis methods are depicted in section 2.5.1. Figure 2 shows the typical cerebral hemodynamics at the surgical and control sides from one patient (12) undergoing CEA. Upon initial clamping of the ICA for removing atheromatous plaque, the rCBF at the surgical side decreased sharply and rapidly (see figure 2(a)), causing immediate reductions in both $\Delta[HbO_2]$ and $\Delta[Hb]$ (see figure 2(b)). These instantaneous responses are expected since the ICA clamping cut off the blood flow (rCBF) and reduced the blood volume (proportional to $[HbO_2]$ + $[Hb]$) supplied to the surgical side of the brain. After reaching its minimal level, rCBF increased and partially recovered toward its baseline value in a short time period although the rCBF level finally remained slightly lower than its pre-ICA baseline (see figure 2(a)). The observed rCBF increase/recovery at the surgical side was likely due to the compensation of blood flow from the control side of the brain (see the rCBF decrease at the control side described in the following paragraph). The instantaneous rCBF increase/recovery temporarily elevated both $\Delta[HbO_2]$ and $\Delta[Hb]$. However, as a result of ICA clamping and continuous cerebral oxygen consumption, $\Delta[HbO_2]$ decreased whereas $\Delta[Hb]$ increased gradually (see figure 2(b)). Following the release of arterial clamping, there was an obvious reactive hyperemia (see figure 2(a)), causing small fluctuations in cerebral oxygenation (see figure 2(b)). Ultimately, the post-CEA rCBF (121.3%) was higher than its baseline value at the surgical side (see figure 2(a)).

The hemodynamic responses to ICA clamping at the control side were different from those at the surgical side; rCBF decreased rapidly at the beginning of clamping and stayed in a
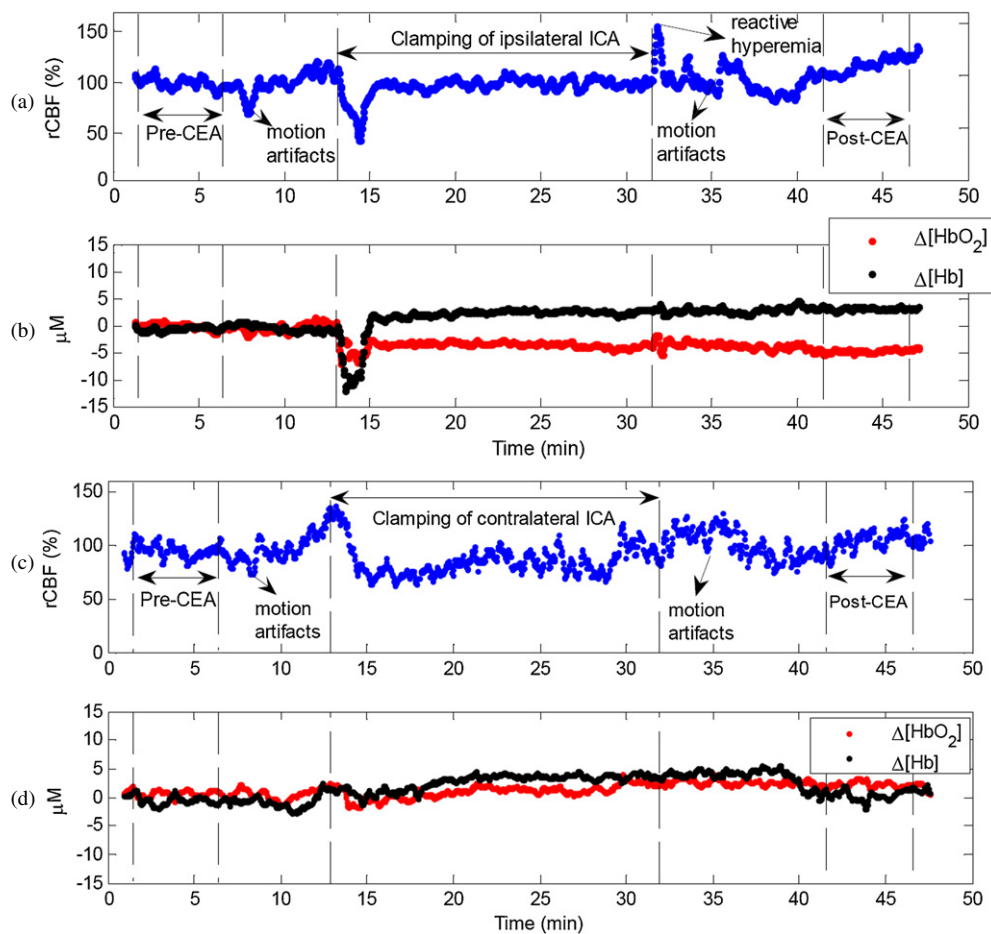
Figure 2. Typical cerebral hemodynamic changes during carotid endarterectomy (CEA). (a) Relative cerebral blood flow (rCBF) and (b) cerebral oxygenation changes ($\Delta[HbO_2]$, $\Delta[Hb]$) at the surgical side; (c) rCBF and (d) $\Delta[HbO_2]$ and $\Delta[Hb]$ at the control side. The vertical dashed lines indicate the beginning and ending of ICA clamping or the periods for calculation of the pre-CEA baseline (5 min) and post-CEA value (5 min). Note that motion artifacts induced by the surgical procedure (e.g., incision, touching vessels, patient position adjustment) may introduce noises to optical measurements. These motion artifacts are marked and corresponding data are excluded in the data analysis.

relatively lower level (compared to its baseline) during clamping (see figure 2(c)) whereas the changes in cerebral oxygenation ($\Delta[HbO_2]$ and $\Delta[Hb]$) were small (see figure 2(d)). The rCBF decrease during clamping at the control side is likely due to the redistribution (compensation) of blood flow to the surgical/clamping side of brain, since this flow decrease was synchronized with the flow increase/recovery at the surgical side (see figure 2(a)). Interestingly, the cerebral oxygenation level at the control side (see figure 2(d)) could be maintained constantly during the arterial clamping even when the rCBF was lower than its baseline level (see figure 2(c)). Finally, the post-CEA rCBF was slightly higher than its baseline value at the control side.
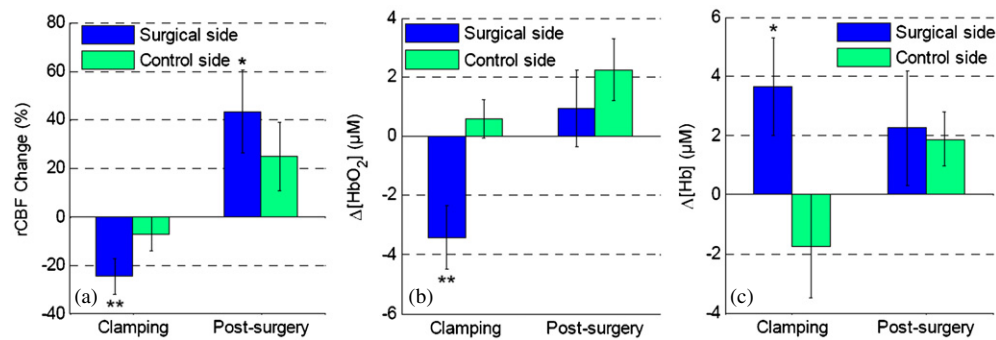
Figure 3. Averaged cerebral hemodynamic changes over all patients during ICA clamping and after CEA (post-surgery). (a) rCBF; (b) $\Delta[HbO_2]$; (c) $\Delta[Hb]$. ** represents $p < 0.01$ and * represents $p < 0.05$. The rCBF and cerebral oxygenation at the surgical sides were significantly altered by ICA clamping. By contrast, there were no significant hemodynamic changes during ICA clamping at the control sides. Significant increases in rCBF after CEA were observed only at the surgical sides. Post-CEA changes in cerebral oxygenation were not significant at both surgical and control sides.

3.2. Averaged hemodynamic changes over patients throughout CEA

The data analysis methods are depicted in section 2.5.2. The averaged results (mean $\pm$ standard error) during ICA clamping and after CEA are summarized in figure 3 over all patients. On average, the rCBF and cerebral oxygenation at the surgical sides were significantly altered by ICA clamping (rCBF $= -24.7 \pm 7.3\%$, $p = 0.006$; $\Delta[HbO_2] = -3.4 \pm 1.1$ μMol, $p = 0.009$; $\Delta[Hb] = +3.6 \pm 1.6$ μMol, $p = 0.049$). By contrast, the hemodynamic changes at the control sides during ICA clamping were not statistically significant (rCBF $= -7.4 \pm 6.9\%$; $\Delta[HbO_2] = +0.6 \pm 0.7$ μMol; $\Delta[Hb] = -1.7 \pm 1.8$ μMol, $p > 0.3$). Significant increases in rCBF ($+43.2 \pm 16.9\%$, $p = 0.03$) after CEA compared to the pre-CEA baseline were observed only at the surgical sides (see figure 3(a)). Post-CEA changes in cerebral oxygenation were not significant at both surgical and control sides (see figures 3(b) and (c)).

3.3. Instantaneous changes in CBF and EEG power during ICA clamping

The data analysis methods are depicted in sections 2.4 and 2.5.3. Figure 4 shows the calculated slope (S), D-index and time-to-minimum for both CBF (top panel) and EEG (bottom panel) data obtained from the surgical side in the same patient (12) presented in figure 2. The large negative CBF slope (-1.25) during the first 30 s clamping period indicates the rapid CBF decrease that resulted from ICA clamping (see figure 4(a)). The time duration of CBF decrease and maximal CBF change during the entire clamping period were characterized by time-to-minimum (80 s) and D-index (-66.2%) (see figure 4(b)). By contrast, the EEG power changed slightly ($S = 0.11$, see figure 4(c)) and reached its minimum (D-index $= -42.8\%$) in a longer period of time (time-to-minimum $= 1016$ s) (see figure 4(d)).

Different patients demonstrated different instantaneous responses to the ICA clamping. Figure 5 illuminates the CBF and EEG responses to ICA clamping at the surgical side in another patient (5). This patient showed relatively large decreases in both CBF ($S = -0.87$) and EEG power ($S = -0.59$) at the beginning of arterial clamping (see figures 5(a) and (c)). The maximal changes in CBF (D-index $= -26.3\%$) and EEG power (D-index $= -27.4\%$)
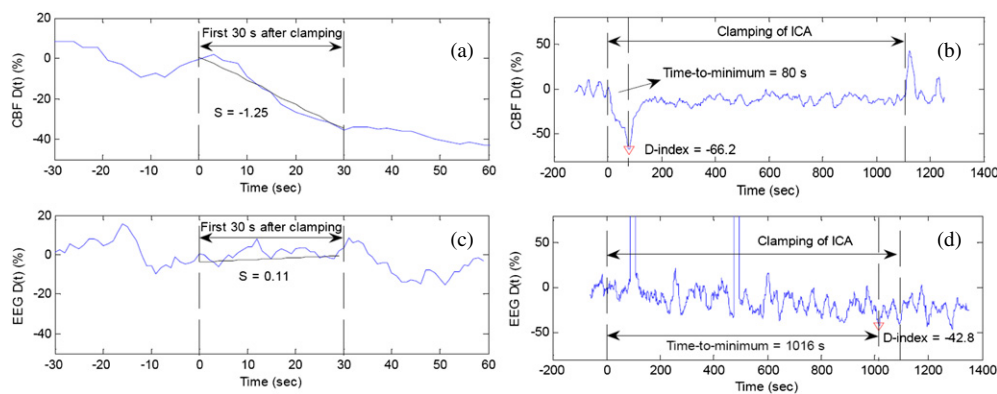
Figure 4. The slope (*S*), *D*-index and time-to-minimum for both CBF (top panel) and EEG (bottom panel) at the surgical side in patient 12. The large negative CBF slope (*S* = −1.25) during the first 30 s clamping period indicates the rapid CBF decrease due to ICA clamping (a). The time duration of CBF decrease and maximal CBF decrease during the entire clamping period was characterized by time-to-minimum (80 s) and *D*-index (−66.2%), respectively (b). By contrast, the EEG power changes were small and slow (*S* = 0.11) (c), and reached its minimum (*D*-index = −42.8%) in a long period of time (time-to-minimum = 1016 s) (d).
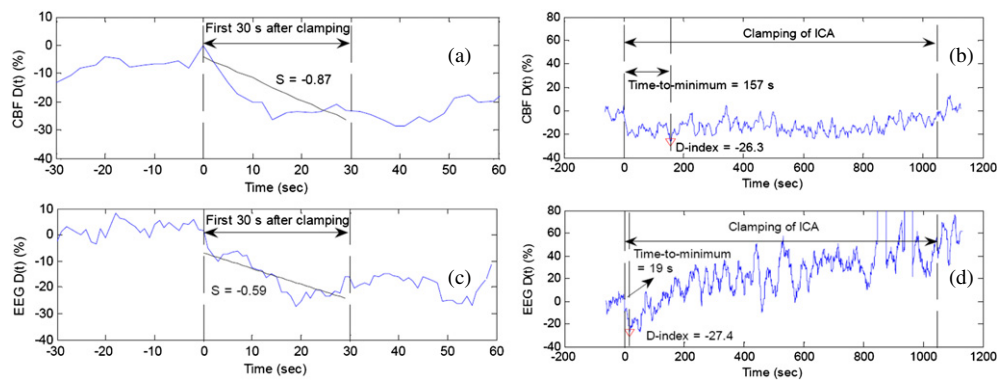
Figure 5. The slope (*S*), *D*-index and time-to-minimum for both CBF (top panel) and EEG (bottom panel) at the surgical side in patient 5. This patient showed relatively large decreases in both CBF (*S* = −0.87) and EEG power (*S* = −0.59) at the beginning of arterial clamping, (a) and (c). The maximal changes in CBF (*D*-index = −26.3%) and EEG power (*D*-index = −27.4%) during the entire clamping period were also similar. However, the time-to-minimums for CBF (157 s) and EEG power (19 s) were quite different, (b) and (d).

were also similar. However, the time-to-minimums for CBF (157 s) and EEG power (19 s) were quite different (see figures 5(b) and (d)).

Figure 6 shows the rCBF and EEG responses to ICA clamping at the surgical sides in most patients (*n* = 11) except patient 8. Most patients showed an expected decrease in EEG power (*D*(*t*)) at the surgical sides during the entire period of ICA clamping. However, the EEG power of patient 8 showed a continuous increase during ICA clamping for unknown reasons (data are not shown). The *D*-index (defined as the minimum of *D*(*t*) during the entire period of ICA clamping) and time-to-minimum (defined as the period from the beginning of ICA clamping to the time of *D*-index) cannot be calculated for this patient since there was no minimum of
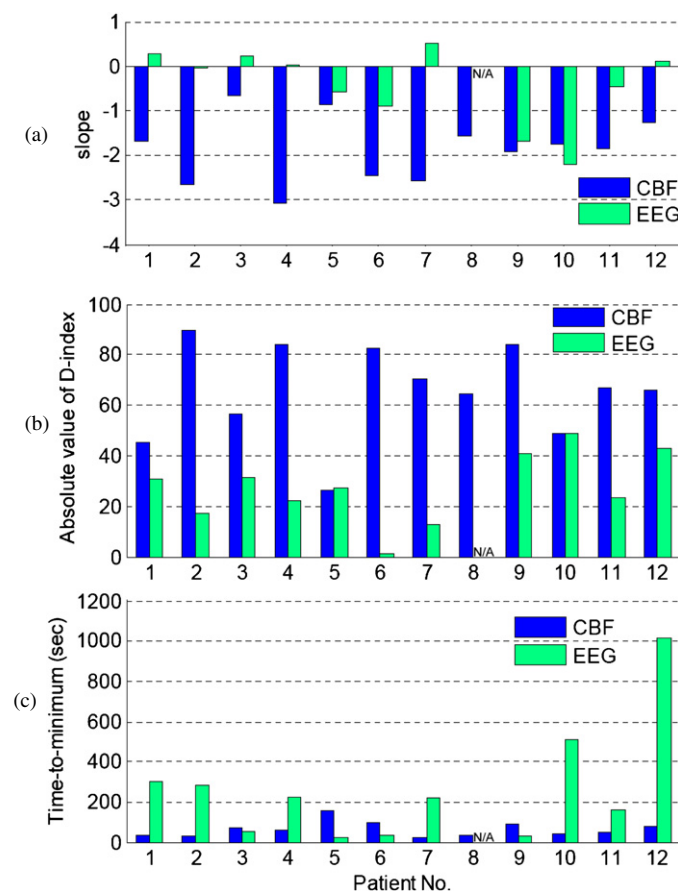
Figure 6. The comparison of CBF and EEG slopes (a), absolute values of the D-index (b), and time-to-minimums (c) in all patients. The data obtained from patient 8 are not applicable (N/A) for comparison due to its paradoxical EEG response. The ICA clamping resulted in large and consistent CBF decreases in all patients ($S = -3.08$ to -0.65). By contrast, the EEG slopes varied ($S = -2.21$ to $+0.51$) and only a few patients ($n = 5$) demonstrated reductions in brain waves ($S < 0$) during ICA clamping. The negative CBF slopes ($n = 11$) were significantly larger ($p = 0.0002$) than the EEG slopes ($n = 11$). The absolute CBF D-indices were significantly higher ($p < 10^{-4}$) than the absolute EEG D-indices. The CBF time-to-minimums were significantly shorter ($p = 0.02$) than the EEG time-to-minimums. These results indicate the higher sensitivity of DCS measurement in detecting cerebral ischemia compared to EEG monitoring.

$D(t)$ (i.e., D-index) during the entire period of ICA clamping. Therefore, the EEG responses in patient 8 were considered as 'paradoxical' and his data were excluded for comparisons, although the clamping-induced CBF responses were in normal ranges ($S = -1.57$, D-index $= -64.3\%$, time-to-minimum $= 33$ s).

As shown in figure 6(a), the ICA clamping resulted in consistent CBF decreases ($S = -3.08$ to -0.65) in all patients at the beginning of ICA clamping, indicating the clamping-induced instantaneous cerebral hypoperfusion. By contrast, the EEG slopes varied from -2.21 to $+0.51$ ($n = 11$), and only a few patients demonstrated reductions in brain waves during the first 30 s clamping period ($S < 0$). The averaged CBF slope (-1.88 ± 0.23) was significantly larger ($p = 0.0002$) than the average EEG slope (-0.44 ± 0.26).

Table 2. Averaged CBF and EEG changes during clamping at the surgical sides over 11 patients.

Parameter	Modality	Mean $\pm$ SE	p value
Slope	CBF	-1.88 ± 0.23	0.0002
	EEG	-0.44 ± 0.26	
Absolute D-index (%)	CBF	65.7 ± 5.9	$<10^{-4}$
	EEG	27.2 ± 4.2	
Time-to-minimum (s)	CBF	66.1 ± 12.0	0.02
	EEG	258.7 ± 88.1	

As illustrated in figure 6(b), the averaged absolute CBF D-index ($65.7 \pm 5.9\%$) was significantly higher ($p < 10^{-4}$) than the absolute EEG D-index ($27.2 \pm 4.2\%$), indicating the higher sensitivity of CBF in detecting the maximal cerebral hypoperfusion.

As demonstrated in figure 6(c), the averaged CBF time-to-minimum (66.1 ± 12.0 s) was significantly shorter ($p = 0.02$) than EEG time-to-minimum (258.7 ± 88.1 s), indicating the earlier CBF response in detecting the most severe cerebral hypoperfusion.

At the 11 control sides, the averaged CBF slope (-0.22 ± 0.30) and absolute D-index ($32.1 \pm 5.5\%$) were significantly smaller ($p < 0.005$) than those ($S = -1.88 \pm 0.23$, absolute D-index $= 65.7 \pm 5.9\%$) at the surgical sides. The CBF time-to-minimum (702.3 ± 115.5 s) was significant longer ($p < 10^{-4}$) than that (66.1 ± 12.0 s) at the surgical sides. By contrast, the averaged EEG slope (-0.45 ± 0.24), absolute D-index ($26.8 \pm 2.2\%$) and time-to-minimum (218.8 ± 40.8 s) were not significantly different from those ($S = -0.44 \pm 0.26$, absolute D-index $= 27.2 \pm 4.2\%$, time-to-minimum $= 258.7 \pm 88.1$ s) at the surgical sides ($p > 0.05$).

Table 2 summarizes the means and standard errors of clamping-induced CBF and EEG responses at the surgical sides over 11 patients, as well as the significant differences (p value < 0.05) between the CBF and EEG responses. Overall, no correlations were found between the CBF and EEG responses at either surgical sides or control sides.

3.4. Clinical outcomes after CEA

All patients had uneventful postoperative course, and there was no late postoperative stroke, myocardial infection or death. Only one patient (11) developed the symptom of headache. Interestingly, this patient exhibited remarkably larger CBF decreases during ICA clamping at both surgical (-62.2%) and control (-55.2%) sides compared to the averaged CBF decreases over all patients at the surgical ($-24.7 \pm 7.3\%$) and control ($-7.4 \pm 6.9\%$) sides. The CBF response to ICA clamping in this patient (11) was faster, greater and earlier compared to EEG response (see figure 6).

4. Discussion and conclusions

Real-time monitoring of cerebral hemodynamic status during CEA provides essential information for reducing the risks of clamping-induced cerebral hypoperfusion/hypoxia (Rowed *et al* 2004) and post-CEA CHS (Adhiyaman and Alexander 2007). At present, most techniques used for monitoring of cerebral perfusion during CEA are limited to indirect estimation of CBF (e.g., EEG, NIRS oximeter, SEP, SP), which may not be consistent with direct CBF measurements. TCD and Xe^{133} techniques are the methods currently used in clinic to directly measure middle cerebral artery blood flow or regional CBF during CEA. It has

been suggested by TCD and Xe^{133} measurements that a substantial CBF reduction ($>\sim 70\%$) during ICA clamping should be considered as a severe cerebral ischemia for selective shunting (Friedell *et al* 2008, Jansen *et al* 1993) and a significant CBF increase ($>\sim 100\%$) after CEA as a risk of CHS (Adhiyaman and Alexander 2007, Sundt *et al* 1981). Unfortunately, TCD can only insonate the proximal portions of the intracranial arteries, which may not be consistent with CBF (Edlow *et al* 2010), and it cannot be performed on 10–15% patients due to the lack of a temporal bone window (Pennekamp *et al* 2009). The requirement of radioactive isotope injection precludes the wide use of Xe^{133} technique in clinic. Other methods such as NIRS tissue oximeter and EEG have also been explored to detect cerebral ischemia for shunting selection. Unfortunately, neither is perfect. The ischemic threshold determined by the NIRS tissue oximeter varies substantially (5–25% reduction in blood oxygen saturation), thus reducing the reliability for shunting decision (Pennekamp *et al* 2009). Although some studies have demonstrated that CEA could be performed by EEG monitoring with stable shunting threshold (e.g., $>50\%$ reduction in alpha-band activities or >0.7 Hz asymmetry of main frequency) (Blume *et al* 1986, Plestis *et al* 1997, Friedell *et al* 2008, Pennekamp *et al* 2009, Hirofumi *et al* 2003), post-surgical neurological deficit or cerebral infarction was still found in some patients with no significant EEG changes during CEA (Rowed *et al* 2004, Jansen *et al* 1993). The unsuccessful probing of severe cerebral ischemia by EEG suggests the need for direct CBF monitoring since the EEG changes originated from the CBF changes. It is well known that the sudden CBF interruption could cause a disruption of neural activity followed by cellular death within a few minutes depending on the residual blood flow and the duration of cerebral ischemia that are not easily measurable in clinical practice (Cursi *et al* 2005).

We have demonstrated in this study that the portable DCS flow-oximeter (see figure 1) can noninvasively and continuously detect the changes in CBF and cerebral oxygenation during CEA, and the optical measurements are very sensitive to physiological events such as ICA clamping and releasing. As expected, ICA clamping resulted in a significant CBF decrease accompanied with cerebral deoxygenation at the surgical sides (see figures 2(a) and (b)). After the ICA stenosis was cleaned and clamping was released, both CBF and cerebral oxygenation recovered gradually toward their baselines, and eventually the post-CEA CBF level was significantly higher than its baseline level. By contrast, the cerebral hemodynamic change during CEA at the control side (see figures 2(c) and (d)) was less than the surgical side, and the cerebral autoregulation/compensation between the two hemispheres was observed.

Note that baseline variations in CBF and oxygenation before ICA clamping were observed in some patients (see an example shown in figure 2), which are not surprising considering the complexity of surgical operations. Many factors could cause the baseline variations in cerebral hemodynamics such as physiological responses (e.g., blood pressure, heart rate) to anesthesia and motion artifacts induced by the adjustment of head position for operation convenience. Although the baseline variations may influence the estimations of individual CBF and cerebral oxygenation changes, the averaged results over patients should reduce such influences. Nevertheless, the ICA clamping-induced significant hemodynamic alterations were clearly observed in all patients involved in this study.

The patients involved in this study showed similar hemodynamic responses throughout the CEA: significant decreases in CBF and cerebral oxygenation during ICA clamping and significant increases in CBF after CEA at the surgical sides; and remarkable but insignificant hemodynamic variations at the control sides (see figure 3). However, different patients demonstrated different sensitivities in response to CEA as indicated by the large error bars shown in figure 3, which are likely dependent on the severity of ICA stenosis, duration of ICA clamping, sensitivity to spontaneous perturbations (e.g., ICA clamping), contralateral

compensation (mainly determined by the integrity of the circle of Willis) and cerebral adaptive capacity. The large rCBF difference between the surgical and control hemispheres ($p = 0.02$) during ICA clamping (see figure 3(a)) might be due to the cerebral impairment in contralateral flow compensation capacity in the patients with severe ICA stenosis (see table 1). Quantification of individual cerebral response to CEA provides useful information for evaluating surgical impacts on brain and for optimizing individual intervention. For example, the clamping-induced cerebral hypoperfusion (CBF decrease) and hypoxia (Δ[HbO$_2$] decrease and Δ[Hb] increase) may cause cerebral tissue damage and/or neural dysfunction if they are severe and long lasting. The CBF elevation after CEA may result from the re-establishment of large arterial blood supply to the ischemic cerebral tissue by CEA as well as the reperfusion after temporary ICA clamping. While the blood supply improvement by CEA is beneficial for patients, the hyperperfusion (e.g., >100% CBF increase) after CEA may cause CHS (Adhiyaman and Alexander 2007). Separation of the CBF improvement from the reperfusion effect requires long-term CBF monitoring, which will be the subject of future work. Nevertheless, intraoperative monitoring of clamping-induced cerebral hypoperfusion and post-CEA-induced reperfusion would help in making decisions to apply acute interventions (e.g., arterial shunting) for avoiding brain tissue damage or to adopt medications for reducing the risk of CHS.

To test the sensitivity of the optical measurements in the detection of instantaneous cerebral hypoperfusion at the early time period of ICA clamping for selective shunting, we employed similar methods on data analysis for both EEG spectrum and CBF (see sections 2.4 and 2.5). Several studies have been performed in human subjects to identify cerebral ischemia during ICA clamping either by on-line visual inspection or by a more sophisticated but objective off-line spectral analysis of EEG signals (Cursi *et al* 2005, Rigamonti *et al* 2005, Blume *et al* 1986). The EEG alpha-band activity modifications during ICA clamping seem to play an important role in determining the dynamics of cerebral ischemia. For example, Cursi *et al* employed continuous EEG monitoring during 47 consecutive CEA to evaluate the usefulness of EEG alpha-band power in detecting cerebral hypoperfusion (Cursi *et al* 2005). Their patients were grouped according to the off-line EEG spectral power changes at the beginning of ICA clamping: group A with major changes, group B with moderate changes and group C with no change. On the basis of on-line visual EEG analysis by expert electroencephalographers, the patients in group A and some patients in group B (with permanent EEG modifications) were shunted. No post-CEA complications were found in all patients with or without shunting ($n = 47$).

According to the established criteria for shunting selection (Cursi *et al* 2005), both on-line visual inspections and off-line power spectral analyses of EEG signals (see figures 4–6) suggest that all patients in the present study do not require arterial shunting during CEA. This is not surprising, as usually only 5–16.8% patients undergoing CEA need arterial shunting (Friedell *et al* 2008, Hirofumi *et al* 2003, Pennekamp *et al* 2009, Nielsen *et al* 2002). Although the lack of selective shunting in the present study makes it impossible to judge the usefulness of CBF measurements for shunting selection, the fact that the CBF responses to ICA clamping in majority of the patients were significantly faster (see figure 6(a)), greater (see figure 6(b)), and earlier (see figure 6(c)) indicates the higher sensitivity of DCS measurement compared to EEG monitoring. The lower sensitivity of EEG measurements is likely anticipated since the clamping-induced interruption of CBF and cerebral oxygenation may or may not significantly affect brain neuronal activity (EEG), which is dependent on each individual response. Considering the difference in detection sensitivity between the DCS and EEG measurements and the small number of patients in this study, it is not surprising that no correlations were found between the CBF and EEG responses to ICA clamping. Moreover, the

observed significant differences between the two hemispheres in CBF slope, *D*-index and time-to-minimum indicate the sensitivity of CBF in distinguishing the ischemic and non-ischemic hemispheres. By contrast, the difference between the two hemispheres in EEG response was not significant.

To conclude, this pilot study demonstrates the capacity of DCS flow-oximeter in detecting cerebral hypoperfusion and hypoxia during ICA clamping and cerebral reperfusion after CEA. DCS provides a direct, objective (without the need of visual inspection), straightforward (without the need of off-line power spectral analysis), and more sensitive way in determining CBF changes compared to EEG. Early detection of the CBF interruption during CEA may alert the surgeons to take prompt actions for preventing consequent complications. Simultaneous monitoring of CBF and cerebral oxygenation (by DCS flow-oximeter) as well as brain neuronal activity (by EEG) provides a comprehensive evaluation of cerebral physiological status during CEA, thus showing a potential for adoption of acute interventions (e.g. shunting, medications) during CEA to reduce the risks of severe cerebral ischemia and CHS. More patients are being recruited and cerebral hemodynamic responses during CEA would be correlated with long-term clinical outcomes (e.g., post-surgical neurological deficit or cerebral infarction) to determine the thresholds of severe hypoperfusion during ICA clamping and hyperperfusion after CEA.

Acknowledgments

References

Ackerstaff R G A, Jansen C, Moll F L, Vermeulen F E E, Hamerlijnck R P H M and Mauser H W 1995 The significance of microemboli detection by means of transcranial Doppler ultrasonography monitoring in carotid endarterectomy *J. Vasc. Surg.* **21** 963–9

Adhiyaman V and Alexander S 2007 Cerebral hyperperfusion syndrome following carotid endarterectomy *Q. J. Med.* **100** 239–44

Belardi P, Lucertini G and Ermirio D 2003 Stump pressure and transcranial Doppler for predicting shunting in carotid endarterectomy *Eur. J. Vasc. Endovasc. Surg.* **25** 164–7

Blume W T, Ferguson G G and Mcneill D K 1986 Significance of EEG changes at carotid endarterectomy *Stroke* **17** 891–7

Boas D A, Campbell L E and Yodh A G 1995 Scattering and imaging with diffusing temporal field correlations *Phys. Rev. Lett.* **75** 1855–8

Boas D A, Gaudette T, Strangman G, Cheng X F, Marota J J A and Mandeville J B 2001 The accuracy of near infrared spectroscopy and imaging during focal changes in cerebral hemodynamics *Neuroimage* **13** 76–90

Boas D A and Yodh A G 1997 Spatially varying dynamical properties of turbid media probed with diffusing temporal light correlation *J. Opt. Soc. Am.* A **14** 192–215

Bond R, Rerkasem K and Rothwell P M 2003 Routine or selective carotid artery shunting for carotid endarterectomy (and different methods of monitoring in selective shunting) *Stroke* **34** 824–5

Bowen J C, Garcia M, Garrard C L, Mankin C J and Fluke M M 1997 Anomalous branch of the internal carotid artery maintains patency distal to a complete occlusion diagnosed by duplex scan *J. Vasc. Surg.* **26** 164–7

Buckley E M 2009 Cerebral hemodynamics in preterm infants during positional intervention measured with diffuse correlation spectroscopy and transcranial Doppler ultrasound *Opt. Express* **17** 12571–81

Chang Y J, Lin S K, Ryu S J and Wai Y Y 1995 Common carotid artery occlusion: evaluation with duplex sonography *Am. J. Neuroradiol.* **16** 1099–105

Chaturvedi S *et al* 2005 Carotid endarterectomy—an evidence-based review. Report of the Therapeutics and Technology Assessment Subcommittee of the American Academy of Neurology *Neurology* **65** 794–801

Cheung C, Culver J P, Takahashi K, Greenberg J H and Yodh A G 2001 *In vivo* cerebrovascular measurement combining diffuse near-infrared absorption and correlation spectroscopies *Phys. Med. Biol.* **46** 2053–65

Cooper R J, Bhatt D, Everdell N L and Hebden J C 2009a A tissue-like optically turbid and electrically conducting phantom for simultaneous EEG and near-infrared imaging *Phys. Med. Biol.* **54** N403–8

Cooper R J, Everdell N L, Enfield L C, Gibson A P, Worley A and Hebden J C 2009b Design and evaluation of a probe for simultaneous EEG and near-infrared imaging of cortical activation *Phys. Med. Biol.* **54** 2093–102

Culver J P, Durduran T, Furuya T, Cheung C, Greenberg J H and Yodh A G 2003 Diffuse optical tomography of cerebral blood flow, oxygenation, and metabolism in rat during focal ischemia *J. Cereb. Blood Flow Metab.* **23** 911–24

Culver J P, Siegel A M, Franceschini M A, Mandeville J B and Boas D A 2005 Evidence that cerebral blood volume can provide brain activation maps with better spatial resolution than deoxygenated hemoglobin *Neuroimage* **27** 947–59

Cursi M, Meraviglia M V, Fanelli G F, Chiesa R, Tirelli A, Comi G and Minicucci F 2005 Electroencephalographic background desynchronization during cerebral blood flow reduction *Clin. Neurophysiol.* **116** 2577–85

Dietsche G, Ninck M, Ortolf C, Li J, Jaillon F and Gisler T 2007 Fiber-based multispeckle detection for time-resolved diffusing-wave spectroscopy: characterization and application to blood flow detection in deep tissue *Appl. Opt.* **46** 8506–14

Duncan A, Meek J H, Clemence M, Elwell C E, Tyszczuk L, Cope M and Delpy D T 1995 Optical pathlength measurements on adult head, calf and forearm and the head of the newborn infant using phase resolved optical spectroscopy *Phys. Med. Biol.* **40** 295–304

Durduran T 2004 Non-invasive measurements of tissue hemodynamics with hybrid diffuse optical methods *PhD Dissertation* University of Pennsylvania, Philadelphia

Durduran T, Yu G, Burnett M G, Detre J A, Greenberg J H, Wang J J, Zhou C and Yodh A G 2004 Diffuse optical measurement of blood flow, blood oxygenation, and metabolism in a human brain during sensorimotor cortex activation *Opt. Lett.* **29** 1766–8

Durduran T *et al* 2009 Transcranial optical monitoring of cerebrovascular hemodynamics in acute stroke patients *Opt. Express* **17** 3884–902

Durduran T *et al* 2010 Optical measurement of cerebral hemodynamics and oxygen metabolism in neonates with congenital heart defects *J. Biomed. Opt.* **15** 10

Edlow B L, Kim M N, Durduran T, Zhou C, Putt M E, Yodh A G, Greenberg J H and Detre J A 2010 The effects of healthy aging on cerebral hemodynamic responses to posture change *Physiol. Meas.* **31** 477–95

Everdell N L, Gibson A P, Tullis I D C, Vaithianathan T, Hebden J C and Delpy D T 2005 A frequency multiplexed near-infrared topography system for imaging functional activation in the brain *Rev. Sci. Instrum.* **76** 093705

Fantini S, Hueber D, Franceschini M A, Gratton E, Rosenfeld W, Stubblefield P G, Maulik D and Stankovic M R 1999 Non-invasive optical monitoring of the newborn piglet brain using continuous-wave and frequency-domain spectroscopy *Phys. Med. Biol.* **44** 1543–63

Farrell T J, Patterson M S and Essenpreis M 1998 Influence of layered tissue architecture on estimates of tissue optical properties obtained from spatially resolved diffuse reflectometry *Appl. Opt.* **37** 1958–72

Fisch B J 1999 *Fisch and Spehlmann's EEG Primer: Basic Principles of Digital and Analog EEG* 3rd edn (Amsterdam: Elsevier)

Franceschini M A, Joseph D K, Huppert T J, Diamond S G and Boas D A 2006 Diffuse optical imaging of the whole head *J. Biomed. Opt.* **11** 054007

Franceschini M A, Nissila I, Wu W C, Diamond S G, Bonmassar G and Boas D A 2008 Coupling between somatosensory evoked potentials and hemodynamic response in the rat *Neuroimage* **41** 189–203

Friedell M L, Clark J M, Graham D A, Isley M R and Zhang X F 2008 Cerebral oximetry does not correlate with electroencephalography and somatosensory evoked potentials in determining the need for shunting during carotid endarterectomy *J. Vasc. Surg.* **48** 601–6

Gagnon L, Desjardins M, Jehanne-Lacasse J, Bherer L and Lesage F 2008 Investigation of diffuse correlation spectroscopy in multi-layered media including the human head *Opt. Express* **16** 15514–30

Hebden J C, Gibson A, Austin T, Yusof R M, Everdell N, Delpy D T, Arridge S R, Meek J H and Wyatt J S 2004 Imaging changes in blood volume and oxygenation in the newborn infant brain using three-dimensional optical tomography *Phys. Med. Biol.* **49** 1117–30

Hirofumi O, Otone E, Hiroshi I, Satosi I, Shigeo I and Masato N Y S 2003 The effectiveness of regional cerebral oxygen saturation monitoring using near-infrared spectroscopy in carotid endarterectomy *J. Clin. Neurosci.* **10** 79–83

Jansen C, Vriens E M, Eikelboom B C, Vermeulen F E, van Gijn J and Ackerstaff R G 1993 Carotid endarterectomy with transcranial Doppler and electroencephalographic monitoring. A prospective study in 130 operations *Stroke* **24** 665–9

Kaiser D A 2005 Basic principles of quantitative EEG *J. Adult Dev.* **12** 99–104

Kienle A and Glanzmann T 1999 *In vivo d*etermination of the optical properties of muscle with time-resolved reflectance using a layered model *Phys. Med. Biol.* **44** 2689–702

Kim J G, Xia M N and Liu H L 2005 Extinction coefficients of hemoglobin for near-infrared spectroscopy of tissue *IEEE Eng. Med. Biol. Mag.* **24** 118–21

Kim M N *et al* 2010 Noninvasive measurement of cerebral blood flow and blood oxygenation using near-infrared and diffuse correlation spectroscopies in critically brain-injured adults *Neurocrit. Care* **12** 173–80

Li J, Dietsche G, Iftime D, Skipetrov S E, Maret G, Elbert T, Rockstroh B and Gisler T 2005 Noninvasive detection of functional brain activity with near-infrared diffusing-wave spectroscopy *J. Biomed. Opt.* **10** 44002

Li J, Ninck M, Koban L, Elbert T, Kissler J and Gisler T 2008 Transient functional blood flow change in the human brain measured noninvasively by diffusing-wave spectroscopy *Opt. Lett.* **33** 2233–5

Mariucci G, Stasi M A, Taurelli R, Nardo P, Tantucci M, Pacifici L, Carminati P and Ambrosini M V 2003 EEG power spectra changes and forebrain ischemia in rats *Can. J. Neurol. Sci.* **30** 54–60

Matic P, Ilijevski N, Radak S, Kolar J and Radak D 2009 Recanalization of chronic carotid occlusion: case report and review of the literature *Vascular* **17** 281–3

Moritz S, Kasprzak P, Arit M, Taeger K and Metz C 2007 Accuracy of cerebral monitoring in detecting cerebral ischemia during carotid endarterectomy *Anesthesiology* **107** 563–9

Nielsen M Y, Sillesen H H, Jorgensen L G and Schroeder T V 2002 The haemodynamic effect of carotid endarterectomy *Eur. J. Vasc. Endovasc. Surg.* **24** 53–8

Oppenheim A V and Schafer R W 1975 *Digital Signal Processing* (Englewood Cliffs, NJ: Prentice-Hall)

Pennekamp C W A, Bots M L, Kappelle L J, Moll F L and de Borst G J 2009 The value of near-infrared spectroscopy measured cerebral oximetry during carotid endarterectomy in perioperative stroke prevention. A review *Eur. J. Vasc. Endovasc. Surg.* **38** 539–45

Plestis K A, Loubser P, Mizrahi E M, Kantis G, Jiang Z D and Howell J F 1997 Continuous electroencephalographic monitoring and selective shunting reduces neurologic morbidity rates in carotid endarterectomy *J. Vasc. Surg.* **25** 620–8

Rigamonti A, Scandroglio M, Minicucci F, Magrin S, Carozzo A and Casati A 2005 A clinical evaluation of near-infrared cerebral oximetry in the awake patient to monitor cerebral perfusion during carotid endarterectomy *J. Clin. Anesth.* **17** 426–30

Roche-Labarbe N, Carp S A, Surova A, Patel M, Boas D A, Grant R E and Franceschini M A 2010 Noninvasive optical measures of CBV, StO(2), CBF index, and rCMRO(2) in human premature neonates' brains in the first six weeks of life *Hum. Brain Mapp.* **31** 341–52

Roche-Labarbe N, Wallois F, Ponchel E, Kongolo G and Grebe R 2007 Coupled oxygenation oscillation measured by NIRS and intermittent cerebral activation on EEG in premature infants *Neuroimage* **36** 718–27

Rovati L, Salvatori G, Bulf L and Fonda S 2007 Optical and electrical recording of neural activity evoked by graded contrast visual stimulus *Biomed. Eng. Online* **6** 1–5

Rowed D W, Houlden D A, Burkholder L M and Taylor A B 2004 Comparison of monitoring techniques for intraoperative cerebral ischemia *Can. J. Neurol. Sci.* **31** 347–56

Shang Y, Zhao Y, Cheng R, Dong L, Irwin D and Yu G 2009 Portable optical tissue flow oximeter based on diffuse correlation spectroscopy *Opt. Lett.* **34** 3556–8

Song Y L, Kim J G, Mason R P and Liu H L 2005 Investigation of rat breast tumour oxygen consumption by hear-infrared spectroscopy *J. Phys. D: Appl. Phys.* **38** 2682–90

Strangman G, Franceschini M A and Boas D A 2003 Factors affecting the accuracy of near-infrared spectroscopy concentration calculations for focal changes in oxygenation parameters *Neuroimage* **18** 865–79

Sundt T M, Sharbrough F W, Piepgras D G, Kearns T P, Messick J M and O'Fallon W M 1981 Correlation of cerebral blood flow and electroencephalographic changes during carotid endarterectomy: with results of surgery and hemodynamics of cerebral ischemia *Mayo Clin. Proc.* **56** 533–43

Tian F H, Chance B and Liu H L 2009 Investigation of the prefrontal cortex in response to duration-variable anagram tasks using functional near-infrared spectroscopy *J. Biomed. Opt.* **14** 054016

van Beekvelt M C P, Borghuis M S, van Engelen B G M, Wevers R A and Colier W N J M 2001 Adipose tissue thickness affects *in vivo* quantitative near-IR spectroscopy in human skeletal muscle *Clin. Sci.* **101** 21–8

Yu G, Durduran T, Lech G, Zhou C, Chance B, Mohler E R and Yodh A G 2005a Time-dependent blood flow and oxygenation in human skeletal muscles measured with noninvasive near-infrared diffuse optical spectroscopies *J. Biomed. Opt.* **10** 024027

Yu G, Durduran T, Zhou C, Wang H W, Putt M E, Saunders H M, Sehgal C M, Glatstein E, Yodh A G and Busch T M 2005b Noninvasive monitoring of murine tumor blood flow during and after photodynamic therapy provides early assessment of therapeutic efficacy *Clin. Cancer Res.* **11** 3543–52

Yu G, Floyd T F, Durduran T, Zhou C, Wang J J, Detre J A and Yodh A G 2007 Validation of diffuse correlation spectroscopy for muscle blood flow with concurrent arterial spin labeled perfusion MRI *Opt. Express* **15** 1064–75

Zhou C *et al* 2007 Diffuse optical monitoring of blood flow and oxygenation in human breast cancer during early stages of neoadjuvant chemotherapy *J. Biomed. Opt.* **12** 051903

Zhou C, Eucker S A, Durduran T, Yu G, Ralston J, Friess S H, Ichord R N, Margulies S S and Yodh A G 2009 Diffuse optical monitoring of hemodynamic changes in piglet brain with closed head injury *J. Biomed. Opt.* **14** 034015

Zirak P, Delgado-Mederos R, Martí-Fàbregas J and Durduran T 2010 Effects of acetazolamide on the micro- and macro-vascular cerebral hemodynamics: a diffuse optical and transcranial Doppler ultrasound study *Biomed. Opt. Express* **1** 1443–59